

MICRO-SEISMOMETERS VIA ADVANCED MESO-SCALE FABRICATION

Caesar T. Garcia, Guclu Onaran, Brad Avenson, Bryan A. Yocom, and Neal A. Hall

Silicon Audio, LLC

Sponsored by the National Nuclear Security Administration

Award No. DE-FG02-08ER85106

ABSTRACT

The Department of Energy (DOE) and the National Nuclear Security Administration (NNSA) seek revolutionary innovations with respect to miniature seismic sensors for the monitoring of nuclear detonations. Specifically, the performance specifications are to be consistent with those obtainable by only an elite few products available today, but with orders of magnitude reduction in size, weight, power, and cost. The proposed commercial innovation calls upon several advanced fabrication methods and read-out technologies being pioneered by Silicon Audio, including the combination of silicon microfabrication, advanced meso-scale fabrication and assembly, and the use of advanced photonics-based displacement / motion detection methods. Early Phase II development has demonstrated 1) verified and repeatable sub $2\text{ng}/\sqrt{\text{Hz}}$ noise floor from 5 to 100Hz, 2) compact integration of 3-axis prototypes and 3) robust deployment exercises. Ongoing developments are focusing on low frequency challenges, low power consumption, ultra-miniature size, and low cross axis sensitivity. Successful implementation will result in a demonstration unit roughly the size of a 9-volt battery with the ability to address advanced national security needs of the DOE/NNSA. Additional applications envisioned include military/defense, scientific instrumentation, oil and gas exploration, inertial navigation, and civil infrastructure monitoring.

| Report Documentation Page | | | Form Approved OMB No. 0704-0188 | |
|---|------------------------------------|---|--|--|
| <p>Public reporting burden for the collection of information is estimated to average 1 hour per response, including the time for reviewing instructions, searching existing data sources, gathering and maintaining the data needed, and completing and reviewing the collection of information. Send comments regarding this burden estimate or any other aspect of this collection of information, including suggestions for reducing this burden, to Washington Headquarters Services, Directorate for Information Operations and Reports, 1215 Jefferson Davis Highway, Suite 1204, Arlington VA 22202-4302. Respondents should be aware that notwithstanding any other provision of law, no person shall be subject to a penalty for failing to comply with a collection of information if it does not display a currently valid OMB control number.</p> | | | | |
| 1. REPORT DATE SEP 2010 | 2. REPORT TYPE | 3. DATES COVERED 00-00-2010 to 00-00-2010 | | |
| 4. TITLE AND SUBTITLE Micro-Seismometers via Advanced Meso-Scale Fabrication | | | 5a. CONTRACT NUMBER | |
| | | | 5b. GRANT NUMBER | |
| | | | 5c. PROGRAM ELEMENT NUMBER | |
| 6. AUTHOR(S) | | | 5d. PROJECT NUMBER | |
| | | | 5e. TASK NUMBER | |
| | | | 5f. WORK UNIT NUMBER | |
| 7. PERFORMING ORGANIZATION NAME(S) AND ADDRESS(ES) Silicon Audio, LLC, 2124 E 6th St Ste 105, Austin, TX, 78702 | | 8. PERFORMING ORGANIZATION REPORT NUMBER | | |
| 9. SPONSORING/MONITORING AGENCY NAME(S) AND ADDRESS(ES) | | | 10. SPONSOR/MONITOR'S ACRONYM(S) | |
| | | | 11. SPONSOR/MONITOR'S REPORT NUMBER(S) | |
| 12. DISTRIBUTION/AVAILABILITY STATEMENT Approved for public release; distribution unlimited | | | | |
| 13. SUPPLEMENTARY NOTES Published in Proceedings of the 2010 Monitoring Research Review - Ground-Based Nuclear Explosion Monitoring Technologies, 21-23 September 2010, Orlando, FL. Volume I. Sponsored by the Air Force Research Laboratory (AFRL) and the National Nuclear Security Administration (NNSA). U.S. Government or Federal Rights License | | | | |
| 14. ABSTRACT <p>The Department of Energy (DOE) and the National Nuclear Security Administration (NNSA) seek revolutionary innovations with respect to miniature seismic sensors for the monitoring of nuclear detonations. Specifically, the performance specifications are to be consistent with those obtainable by only an elite few products available today but with orders of magnitude reduction in size, weight, power, and cost. The proposed commercial innovation calls upon several advanced fabrication methods and read-out technologies being pioneered by Silicon Audio, including the combination of silicon microfabrication, advanced meso-scale fabrication and assembly, and the use of advanced photonics-based displacement / motion detection methods. Early Phase II development has demonstrated 1) verified and repeatable sub 2ng/&#8730;Hz noise floor from 5 to 100Hz, 2) compact integration of 3-axis prototypes and 3) robust deployment exercises. Ongoing developments are focusing on low frequency challenges, low power consumption ultra-miniature size, and low cross axis sensitivity. Successful implementation will result in a demonstration unit roughly the size of a 9-volt battery with the ability to address advanced national security needs of the DOE/NNSA. Additional applications envisioned include military/defense, scientific instrumentation, oil and gas exploration inertial navigation, and civil infrastructure monitoring.</p> | | | | |
| 15. SUBJECT TERMS | | | | |
| 16. SECURITY CLASSIFICATION OF: | | | 17. LIMITATION OF ABSTRACT Same as Report (SAR) | 18. NUMBER OF PAGES 9 |
| a. REPORT unclassified | b. ABSTRACT unclassified | c. THIS PAGE unclassified | | |
| 19a. NAME OF RESPONSIBLE PERSON | | | | |

OBJECTIVES

The DOE/NNSA seeks revolutionary innovations with respect to miniature seismic sensors for the monitoring of nuclear detonations. Specifically, the performance specifications are to be consistent with those obtainable only by a few elite products available today, but with orders of magnitude reduction in size, weight, power, and cost. The specific sensor specifications solicited are as follows:

- Size – less than 1 in³
- Power – less than 100 mW
- Sensor self noise – below USGS NLNM, or approximately 0.5 ng/ $\sqrt{\text{Hz}}$
- Dynamic range at least 120 dB over a frequency band of 0.2 to 40 Hz.

In a prior review (Hall, 2008), we summarized basic design considerations for any proposed technology aiming to meet the aforementioned specifications. In particular, it was shown that meeting the noise requirement demands both a) ultra-low thermal mechanical noise from the seismometer proof mass, and b) high resolution displacement measuring capability of the proof mass motion. As an example, a design with a 2 gram proof mass and 50 Hz open loop resonant frequency may be considered. In this case, achieving the required 0.5 ng/ $\sqrt{\text{Hz}}$ acceleration noise requires a resonance quality factor, Q , of 100 and an ultra-low displacement resolving capability of 50 fm/ $\sqrt{\text{Hz}}$ (Hall, 2008). The high resonance Q , in-turn, requires the use of closed-loop feedback altered dynamics to realize the desired flat frequency response of the sensor. This discussion provides the motivation for Silicon Audio's proposed design innovation, which calls upon advanced meso-scale fabrication of mechanical proof-mass elements, photonics-based displacement / motion detection, micro-scale optoelectronic integration, and the integration of closed-loop sensing modalities for high stability and high dynamic range. In subsequent sections, results are presented which demonstrate this approach.

Sensor Schematic

Phase I prototypes demonstrated the viability of a sensor system similar to that shown in Figure 1. The present design, which has been field tested and demonstrates sub 2ng/ $\sqrt{\text{Hz}}$ noise, is summarized in the following figure.

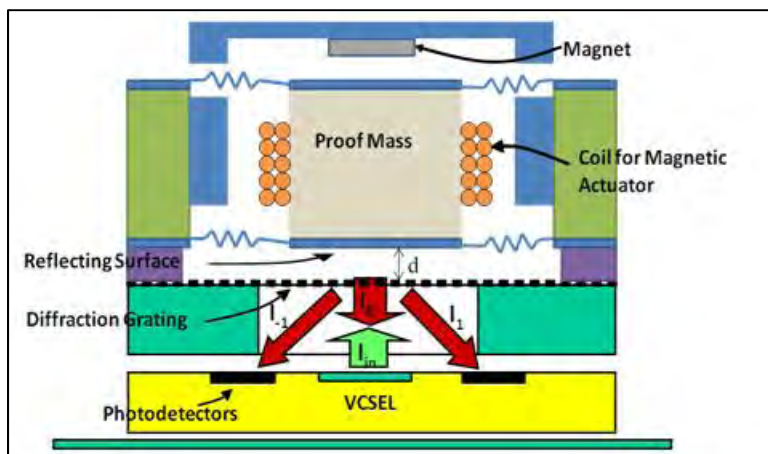


Figure 1. Schematic of a photonics based motion detection principle in development. Light from a semiconductor laser such as a vertical cavity surface emitting laser (VCSEL) illuminates a diffraction grating fabricated on silicon. A portion of the incident light reflects directly off of the grating fingers, while the remaining light travels in between the grating fingers and to the proof mass and back to accrue additional phase. A diffracted field results consisting of a zero and higher orders whose angles remain fixed, but whose intensities are modulated by the relative distance between the proof mass and grating with the sensitivity of a Michelson type interferometer.

A sensing method very similar to that summarized in the caption of Figure 1 has been demonstrated and described in detail in prior developments (Lee et al., 2004; Hall et al., 2007; Hall, et al., 2008). The diffraction grating in this

system serves the function of an optical beamsplitter, directly reflecting half of the incident light while passing the remaining half to travel to the proof-mass and back to accrue additional phase. Being an optical interference based approach, the displacement resolving capability of the method is of very high fidelity – on the order of $20 \text{ fm}/\sqrt{\text{Hz}}$ when using small $500\mu\text{W}$ semiconductor lasers. The intrinsic open loop dynamic range of this approach (i.e., clip level) is limited to approximately $\lambda/4$, where λ is the optical wavelength. This corresponds to the peak-to-trough range of an interference cycle (i.e., fringe cycle) and is approximately 212 nm for an 850 nm wavelength semiconductor laser. Considering that 20 fm displacement can be resolved over a 1 Hz bandwidth, the intrinsic dynamic range is then 140 dB. Over the 40 Hz measurement bandwidth of interest, the open-loop dynamic range is 124 dB.

It is important that the interferometer be operated at a point of quadrature (i.e., a point of maximum slope and linearity on the interference curve). Figure 2 helps to clarify this by summarizing the theoretically predicted relationship between light intensity of the diffracted beams labeled in Figure 1 vs. the gap distance “d” also labeled in Figure 1. The center beam modulation is complementary to the sum of the exterior beams. Therefore, one can use the difference signal (in practice this is done by simple photocurrent subtraction), as the seismometer output signal. The linear operating region is highlighted in the figure. The slope of this curve is the displacement sensitivity of the detection method (after amplification through a photocurrent-to-voltage amplifier, the unit of the y axis is volts, and the sensitivity is therefore expressed in V/m).

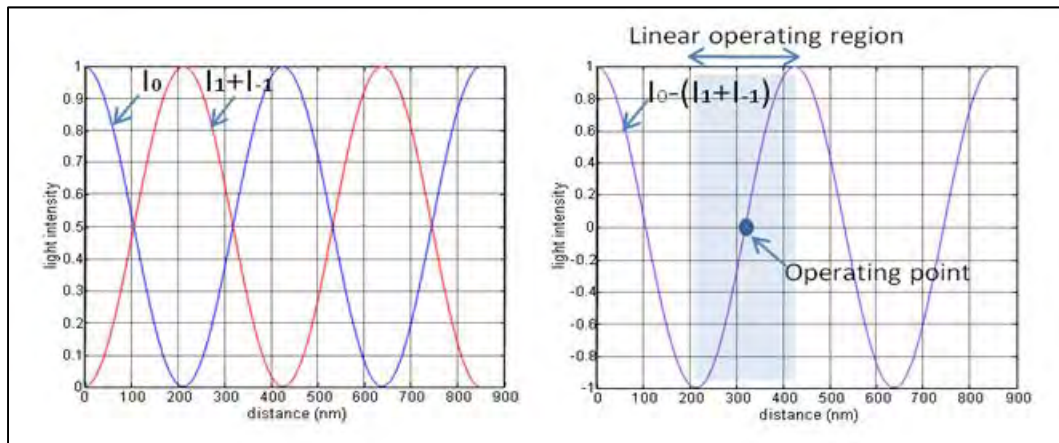


Figure 2. (left) Theoretically predicted relationship between the diffracted beams labeled in Figure 2 vs. gap distance “d” labeled in Figure 2. **(right)** The difference signal is then used to detect the proof mass motion within a single interference fringe.

Operation about a point of quadrature (i.e., the operating point labeled in Figure 2) is maintained by direct actuation of the proof mass using magnetic actuation. In addition, dynamic actuation of the proof mass also enables closed-loop measurement modalities. Closed loop operation is critical in high performance accelerometers, as the high Q of the open loop system required for low thermal noise must be electronically compensated for via feedback-altered-dynamics to achieve the desired flat frequency response (Liu and Kenny, 2001).

RESEARCH ACCOMPLISHED

In this report we present work related to mechanical and optical design optimization and demonstration of small (coke can size), fully integrated, 3-component sensor prototypes with $2\text{ng}/\sqrt{\text{Hz}}$ noise floor.

Design of Mechanical and Optical Systems

Using finite element analysis (FEA), a model has been constructed to analyze the mechanical aspects of the system. This model, shown in Figure 3, was first used to extract the higher order modes of the spring-mass system. These higher modes can become problematic for two reasons. First, it can be shown that cross axis sensitivity is adversely affected by these modes which tend to rock and respond to off-axis excitation. Secondly and perhaps less obviously, higher order modes limit the achievable bandwidth of the closed loop system and pose challenging demands on

closed loop stabilization circuitry¹. By pushing these modes to higher frequencies, away from the fundamental mode of interest, these two problems can be overcome. Several iterations of spring design led to the current 4-arm structure shown. Using FEA tools, the frequencies of problematic higher order modes discovered in Phase I prototypes were positioned from a factor of 5 to a factor of 65 times the fundamental mode of interest.

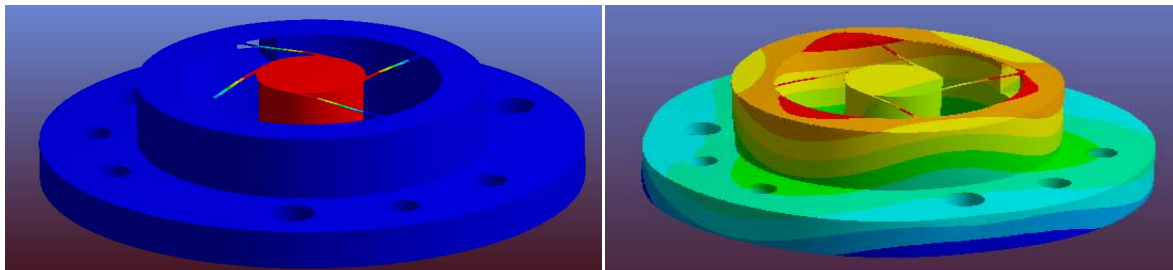


Figure 3. (left) FEA modal analysis used to isolate fundamental mode from higher order modes by a factor of 65. **(right)** FEA thermal analysis simulating temperature induced proof mass deflection.

A second FEA analysis studied the effects of temperature on low frequency signal drift which is believed to be the dominant source of $1/f$ noise. Sensitivity of a Michelson Interferometer depends on both wavelength, λ , and gap distance, d , labeled in Figure 1. Because both of these parameters are subject to change with temperature, it is possible to null out their effects on sensitivity by setting $\Delta d/d = \Delta\lambda/\lambda$ where Δ indicates a temperature induced change. The values of λ and $\Delta\lambda$ are provided by VCSEL manufacturers, and d is a known design parameter, approximately $25\mu\text{m}$. Solving the relationship above leads to a desired Δd value on the order of $1\text{nm}/^\circ\text{C}$. FEA modeling of earlier designs predicted Δd values near $100\text{nm}/^\circ\text{C}$ while the newer 4-arm design predicts a much improved value of approximately $10\text{nm}/^\circ\text{C}$ with future designs anticipated to go even lower. In practice, the easiest way to measure the effectiveness of this design approach is to monitor the coil actuation signal as a function of temperature since this signal is tasked with compensating for any sensitivity drift left uncancelled. Experiments are presently underway to verify the effectiveness of this design.

Equally valuable insight into the optical system is gained by rigorous modeling efforts using custom Fourier Optics based simulations in combination with off the shelf ray-tracing optical modeling CAD tools. OSLO ray-tracing optical modeling software package was used to construct an accurate model of the complete optical system, including a diverging Gaussian source and monochromatic aberrations of lenses. Results from these simulations led to the conclusion that initial estimations of the focal plane location based on first order paraxial approximations were off by 15% leading to less than optimal tolerance to misalignment and optical surface flatness resulting in reduced modulation efficiency. Critical components of the CAD model are labeled in Figure 4.

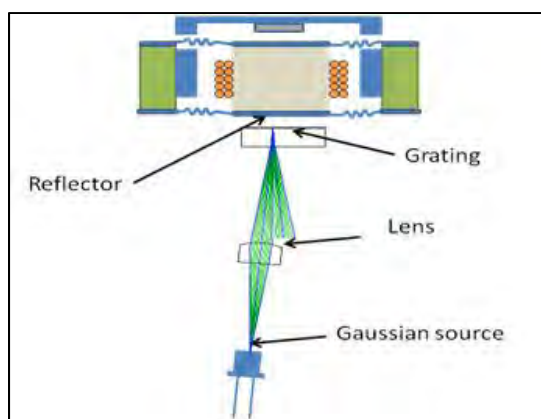


Figure 4: Computer aided optical modeling software improves upon first order paraxial assumptions by 15% to provide accurate focal plane prediction.

¹ Higher order modes can vibrate 180 degrees out of phase with the fundamental mode of interest. When doing so, they confuse the sign of gains in the proportional, integral, and derivative blocks of the proof mass control. This, in turn, can lead to positive rather than negative feedback which causes instability.

Detailed interactions of incident light with the grating/reflector/proof-mass sub-system cannot be studied with macro ray-tracing tools. A custom Fourier Optic diffraction simulation code was developed in Matlab for this purpose. This code, unlike the previous diffraction simulation mentioned in prior reviews (Garcia, 2009; Hall, 2008), was designed to account for relative tilt between grating and reflector planes as well as their absolute separation, d (labeled in Figures 1 and 5 (left)). The goal of these simulations is to generate sensor designs that maintain high optical modulation efficiency, which is defined by the peak-to-trough swing resulting from interference in the diffracted beams. Higher modulation efficiency yields higher output sensitivity and lower sensor self noise. The theoretical curves in Figure 2 display a modulation of 100%. In practice, achieving high modulation efficiency requires careful design.

Variables affecting modulation efficiency are highlighted in Figure 5 (left). These include incident beam angle, β , reflector tilt angle, α , and stand-off distance between the grating surface and the reflector, d . This stand-off, d , is also highlighted in the complete sensor schematic of Figure 1. Another important variable is the numerical aperture of the system, which is a measure of the cone angle of the incident beam focused onto the plane of the diffraction grating. The incident beam at the plane of the grating is focused, but because of the finite stand-off, d , and finite cone angle, the reflector plane is not illuminated with a focused beam. This is addressed in our model by defining a virtual source behind the reflector. Simulation results are presented in Figure 5 (right) for a fixed angle of incidence ($\beta = 2.5^\circ$) and a fixed cone angle of 5° full width at half maximum (FWHM). The contours represent various levels of modulation efficiency, 0.9 being the best defined in the figure and 0.1 being the worst. The modulation efficiency ratio is seen to be a function of α and d .

The choice of distance d is influenced by mechanical criteria in addition to optical design criteria. For example, d affects the damping dynamics of the proof mass structure due to squeeze film effects. For fixed d , the simulation results allow one to study the effect of reflector tilt on modulation ratio. The black solid lines in Figure 5 (right) highlight another fundamental design constraint, namely, the reflector should not touch the grating surface. For example, for a reflector diameter equal to 3mm, all possible designs lie to the right of the solid line in the figure. Understanding from this modeling is critical in prototyping and also in studying manufacturing and assembly tolerances in production.

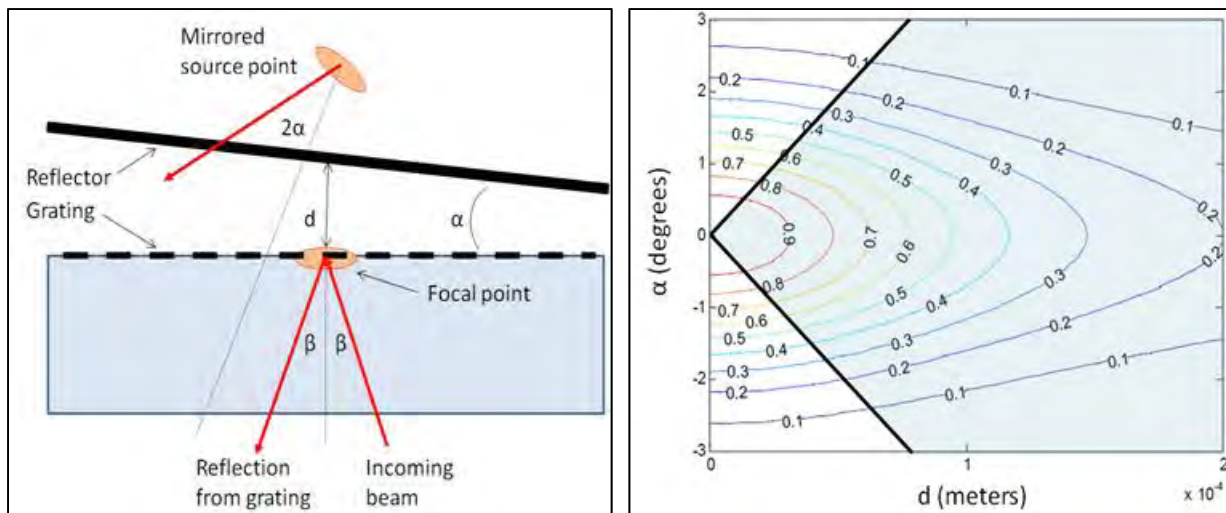


Figure 5. (left) Schematic illustrating relevant tilt angles. (right) Typical result assuming 2.5° incident beam angle (β) and cone angle of 5° FWHM showing contour lines of constant modulation ratio. In this figure a 3mm diameter reflector will limit access to the shaded region of the plot.

Field Testing of Three Axis Prototypes

Silicon Audio has successfully built and tested several 3-axis prototypes. These beta prototypes were designed to demonstrate the current state of the development effort and to address unanticipated challenges associated with building and testing a 3-axis seismometer. The compact design is roughly the size of a 12-oz coke can and incorporates a Galerkin sensor orientation, semi-closed loop force feedback operation, automatic mass centering, and clip level stabilization. In Figure 6, a CAD image (left) is shown along with an actual photograph (right) of the field tested “GeoLight” prototype.

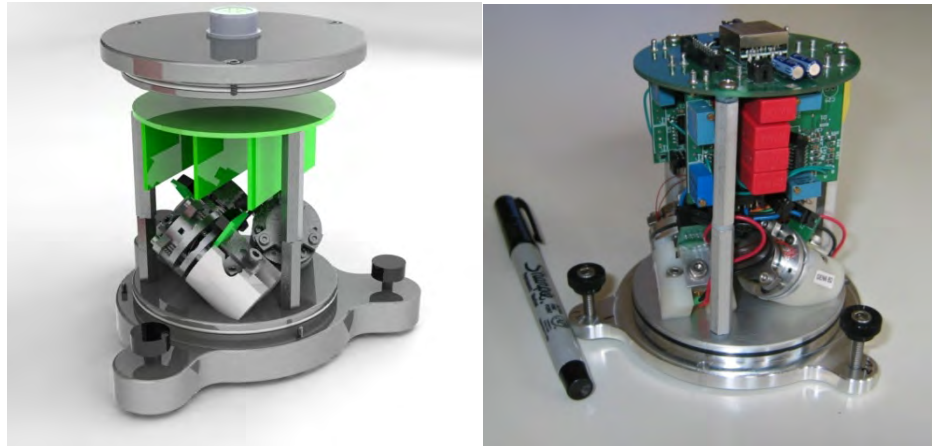


Figure 6. (Left) CAD image of GeoLight prototype along with (right) actual field tested prototype.

Prior to field testing, frequency response measurements of single axis sensors were measured (see Figure 7). In this measurement an excitation signal is provided using the sensor's magnetic coil input while the output signal is detected optically. This measurement highlights a useful self-test capability that can be performed in-situ to monitor each device's frequency response. In addition to testing sensor dynamics, large force excitations can be used to traverse multiple interference fringes (see Figure 2), which enable absolute displacement sensor calibration owing to the fixed optical wavelength. The flattened response is attributed to closed-loop feedback altered dynamics which are summed together with the external excitation signal at the coil input (see Garcia, 2009). Here, the Q factor is reduced from roughly 100 down to critical damping.

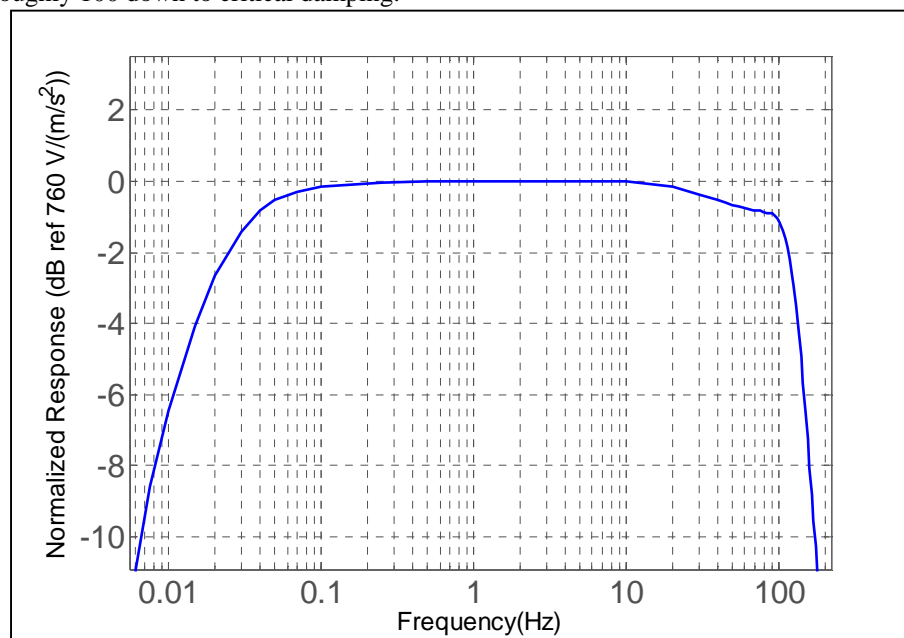


Figure 7: Frequency response measured using magnetic coil self excitation and optical detection capabilities.

During a field test at the USGS Albuquerque Seismology Laboratory (ASL), these prototypes were tested alongside a calibrated Stekheisen STS-2 broadband seismometer. Both instruments were connected to a Quanterra digitizer sampling at 200 Hz and left to record data overnight. Sensor noise floor was assessed using data captured during a non-event period. Initial results, summarized in Figure 8, reveal that at frequencies greater than 3Hz the GeoLight prototype accurately resolves the 2ng/vHz background noise of the test site (e.g., -154 dB level in Fig x). Below 3Hz, $1/f$ noise begins to dominate. Still, the early stage prototype is able to resolve a portion of the microseism peak between 0.1-0.3Hz, at a level of -130 dB or approximately 20ng/vHz .

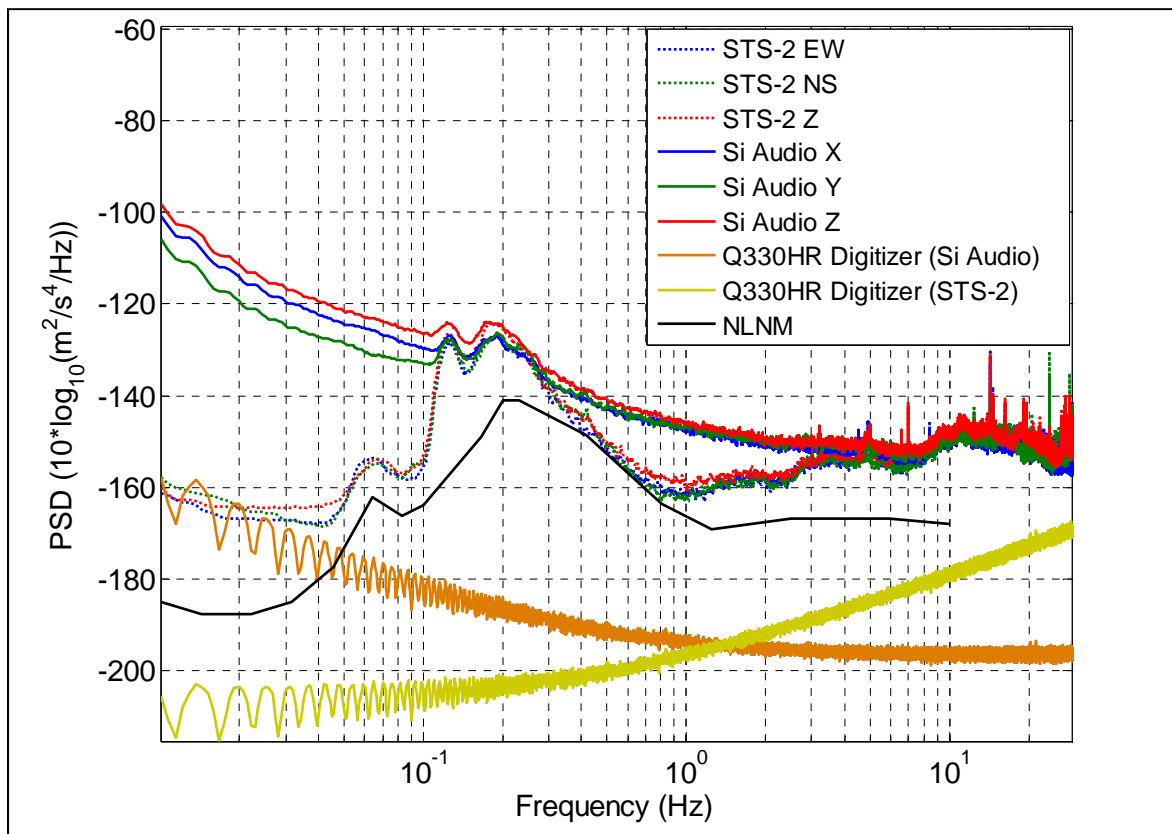


Figure 8: Noise measurement made during visit to USGS ASL demonstrating Silicon Audio's miniature 3-axis GeoLight prototype detecting down to site noise at 3 Hz and above and capturing portions of the 0.2 Hz microseism. Sources of $1/f$ noise at lower frequencies are presently being addressed. For comparison, the NLNM is included as are the digitizer noise levels.

During overnight noise testing, an earthquake originating off the coast of Tarapaca, Chile (UTC 2010/05/06 02:42:47) was recorded. The velocity waveforms of the P-wave arrival are plotted in Figure 9. Excellent matching among all 3 axes can be seen between the GeoLight prototype and the STS-2 calibrated reference.

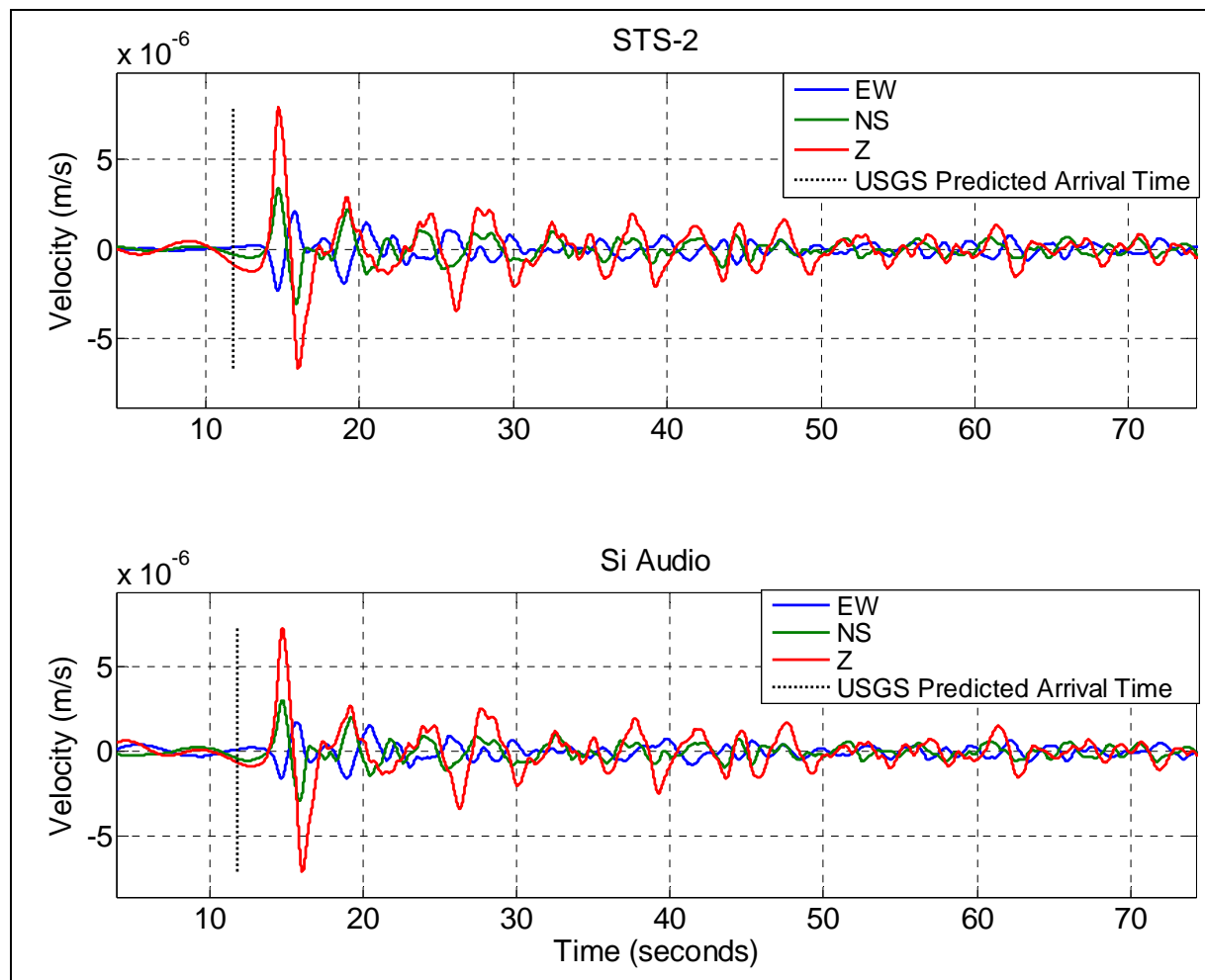


Figure 9: P-wave arrival of Tarapaca, Chile event recorded by STS-2 and by Silicon Audio's GeoLight prototype during testing visit to USGS ASL, May 3-6th 2010.

CONCLUSIONS AND RECOMMENDATIONS

Silicon Audio is addressing the NNSA's rigorous seismometer specifications using an approach that combines silicon micromachined optical elements, integrated semiconductor lasers, photo detection electronics, and meso-scale proof mass structures. This review article focused on a grating based implementation and significant accomplishments were discussed; improved dynamic and optical modeling capabilities, and demonstration of 3-axis prototypes. Future developments will focus primarily on improved noise performance in the 100mHz-5Hz band, low power operation <100mW, and further miniaturization. We envision complete units integrated into a 3-axis sensor package roughly the size of a 9-volt battery.

ACKNOWLEDGEMENTS

The authors graciously thank the NNSA and the DOE SBIR program for support. We also thank the University of Texas, Institute of Geophysics for assistance with Phase I and Phase II field test demonstrations. Finally, we would like to thank Bob Hutt and his team at the USGS Albuquerque Seismology Lab for their assistance with Phase II field testing.

REFERENCES

- Hall, N. A. (2008). Micro-seismometers via advanced mesoscale fabrication, in *Proceedings of the 30th Monitoring Research Review: Ground-Based Nuclear Explosion Monitoring Technologies*, LA-UR-08-05261, Vol. 1, pp. 610–614.
- Hall, N. A., M. Okandan, R. Littrell, B. Bicen, and F. L. Degertekin (2007). Micromachined optical microphones with low thermal-mechanical noise levels, *J. Acous. Soc. Am.* 122 (4): 2031–2037.
- Hall, N. A., M. Okandan, R. Littrell, D. K. Serkland, G. A. Keeler, and K. Peterson (2008). Micromachined accelerometers with optical interferometric read-out and integrated electrostatic actuation, *J. Microelectromech. Syst.* 17 : (1), 37–44.
- Hobbs, P. C. D. (1997). Ultrasensitive laser measurements without tears, *Applied Optics* 36: (4): 903–920.
- Lee, W., N. A. Hall, et al. (2004). Fabrication and characterization of a micromachined acoustic sensor with integrated optical readout. *IEEE Journal on Selected Topics in Quantum Electronics* 10: (3), 643–651.
- Liu, C. H. and T. W. Kenny (2001). A high-precision, wide-bandwidth micromachined tunneling accelerometer, *J. Microelectromech. Syst.* 10: (3) 425–433.
- Garcia, C. T., Onaran, G., Avenson, B., Ellis, M., and N. A. Hall (2009). Micro-Seismometers via Advanced Mesoscale Fabrication. in *Proceedings of the 2009 Monitoring Research Review: Ground-Based Nuclear Explosion Monitoring Technologies*, LA-UR-09-05276, Vol. 1, pp. 330–337.